

**Mixing in 3-D Cavity by Moving Cavity Walls**  
**by Alex Povitsky**  
**Department of Mechanical Engineering**  
**University of Akron, Akron, OH USA**

**Abstract**

The mixing in this enclosure is investigated numerically using 3-D flow in cubical cavity as a geometrically simple model of various natural and engineering flows. The mixing rate is evaluated for several representative scenarios of moving cavity walls: perpendicular motion of top and bottom cavity walls (Case A), motion of the top wall in its plane along its diagonal (Case B1), the top wall in motion to the right while the left vertical wall is in down motion (Case B2), and the top and bottom walls in motion either in parallel directions (Case B3) or in opposite directions (Case B4). The intensity of mixing for the considered cases was evaluated for (i) developing cavity flow initially at rest, which is started by the impulsive motion of cavity wall(s), and (ii) injection of two fluids into the developed cavity flow. For both cases, the initial interface of the two mixing fluids is a horizontal plane located at the middle of the cavity. The mixing rates are compared to the benchmark case in which the top cavity wall moves along its side (Case C). The effects of three-dimensionality of cavity flow on the mixing rate are discussed. The mixing rates are ranked from fastest to slowest in the order B2, B4, A, B1, C, and B3 for developing flow and A, B4, C, B1, B2, and B3 for developed flow.

**Introduction**

Because of the variety of natural, industrial and biomedical prototype applications, steady-state 2-D cavity flows have been widely studied by both experimental and numerical investigations<sup>1</sup>. Studies of 3-D cavity flows started after the pioneering experimental work<sup>2</sup>. However, very few studies have been conducted on the unsteady flow establishment and mixing phase<sup>3,4</sup>. Ref<sup>5</sup> quantifies the mixing characteristics of a two-dimensional, lid-driven blinking Stokes flow ( $Re < 1$ ) to evaluate fluidic components that are critical parts of micro- and nano-scale systems. The latter can be used for detecting both chemical and biological agents and explosives, monitoring the environment for hazardous chemicals or toxins, and diagnosing and treating medical problems. These fluidic components can be used for transporting and mixing small amounts of materials that are subsequently analyzed or delivered to predetermined sites. The above listed applications

include fluid dynamics in small channels that have etched or engraved geometric features, such as grooves<sup>5</sup>.

The goal of this study is to quantify and compare mixing rates in 3-D cubical cavity for developed and developing flowfield for several representative cases of moving cavity walls. By Ref<sup>1</sup>, recirculating cavity flows generated by the motion of one or more of the containing walls are not only technologically important, but they are also of great scientific interest because they display almost all fluid mechanical phenomena in the simplest of geometrical settings. By computational results obtained in the current study, some set-ups of moving walls for cavity flow exhibit relatively slow mixing compared to other configurations that mix well. Each case introduces its degree of three-dimensionality ranking from nearly 2-D flow (with the exception of end walls) to essentially 3-D flow with enhanced mixing.

The normalized variance of concentration is appropriate to evaluate mixing (see<sup>4-6</sup> and references therein). From an initially unmixed state, the variance of concentration decreases over time, indicating that mixing has occurred to a required degree. The current study compares cubical cavity flows configurations caused by motion of cavity wall(s) (see Fig. 1) in order to evaluate the dynamics of variance of concentration and to explain physical reasons for delay in mixing in certain areas of flowfield. In particular, it will be shown in the current study that if the mixing time is sufficient, then the 3-D flow<sup>6</sup> (Case A in Fig. 1a) is driven by the perpendicular motion of top and bottom cavity walls. This thesis, which has recently been proposed by the author, ensures the most completed mixing compared to other configurations of moving cavity wall(s). For Case A,

the axes of primary vortices are in the  $x$  and  $z$  perpendicular directions, which makes the flowfield three-dimensional.

The cubic cavity flow in which the top wall moves in its plane along its diagonal was introduced by the author<sup>7</sup> (Case B1 in Fig.1b). The prototype flows are those typical for urban air pollution<sup>8</sup> and pneumatic transport of powder materials<sup>9</sup>. Refs<sup>10,11</sup> propose the 3-D cavity flow in which the top wall moves to the right, while the left vertical wall moves down with the same constant velocity (see Fig.1c, case B2). For Case B2, the flows recirculate in upper and lower cavity prisms, which are separated by the cavity diagonal plane that forms the plane of symmetry.

The prior study<sup>12</sup> modeled flows in 2-D cavities in which the top and bottom walls move either in the same direction or in opposite directions with the same speed. Different shapes and sizes of streamline patterns were obtained<sup>12</sup> for various values of Reynolds numbers and cavity aspect ratios. The 3-D extension of this motion is introduced<sup>13</sup>. In the current study, the mixing pattern is evaluated for 3-D cavity with its top and bottom moving. For Case B3 (Fig. 1d), the top and bottom walls move in a parallel fashion. For Case B4 (Fig. 1e), the top and bottom walls are in reverse motion.

For Case C (Fig. 1f), the flow inside the cavity is generated by the translation of one cavity wall referred to as the moving lid. This particular configuration is called a lid-driven cavity (LDC)<sup>2</sup> and is widely used for validation of numerical methodologies. It should be noted that cases B2-B4 and C can be reduced to their 2-D analogues, while cases A<sup>6</sup> and B1<sup>7</sup> are essentially three-dimensional,

and do not have their 2-D counterparts. Nevertheless, the current study shows that three-dimensional effects on mixing are significant for cases B2-B4 and C.

To evaluate the time interval for cavity flow development<sup>5</sup>, the variance of concentration as a function of time was computed for  $T \leq 30$ , in which time is normalized by the ratio of the cavity size to moving lid speed,  $L/U$ . By physical experiments,<sup>3</sup> the cavity flowfield was recorded at regular dimensionless time steps:  $\Delta T = 1$ , for  $0 \leq T \leq 12$ . The cavity reached a quasi-steady state by  $T = 8-10$ , which was measured by the stagnation of vortex-core positions, secondary eddy sizes, and velocity profiles.

To extend the cavity flow studies to non-Newtonian fluids, the authors<sup>14</sup> investigated the circulating flow of power-law fluids inside a square cavity for both the parallel and reverse motions of two facing lids. During the parallel motion of the lids, there are two counter-rotating primary vortices, and the streamlines in one half of the cavity is the mirror image of the other with respect to the line  $y/H = 0.5$ . During anti-parallel wall motion, a single primary vortex develops in the cavity. In the future, the current comparative evaluation of intensity of mixing for various 3-D cavity flows can be extended to non-Newtonian flows typical for polymer engineering, food processing, dynamics of drilling fluid, and the manufacture of energy materials.

The study is composed as follows: the mathematical description of fluid motion in 3-D cavity, numerical methodology for the solution of the mathematical model, and methodology for computing the dynamics of variance of concentration are given in Section 2. Computational results of the integral evaluation of mixing rate, local features of flowfield, and mixing in the middle vertical section for each case are presented in Section 3. In Section 4, the 3-D effects on flowfield

and mixing, including finiteness in the span-wise direction for each case, are discussed. Conclusions are presented in the last section.

## 2. Numerical model, grid convergence and evaluation of mixing rate

The governing equations are the three-dimensional transient incompressible continuity and Navier-Stokes equations in Cartesian coordinates  $(x, y, z)$  describing conservation of mass and momentum.

$$\frac{\partial u}{\partial x} + \frac{\partial v}{\partial y} + \frac{\partial w}{\partial z} = 0,$$

(1)

$$\frac{\partial u}{\partial t} + u \frac{\partial u}{\partial x} + v \frac{\partial u}{\partial y} + w \frac{\partial u}{\partial z} + \frac{\partial p}{\partial x} - \frac{1}{Re} \nabla^2 u = 0,$$

$$\frac{\partial v}{\partial t} + u \frac{\partial v}{\partial x} + v \frac{\partial v}{\partial y} + w \frac{\partial v}{\partial z} + \frac{\partial p}{\partial y} - \frac{1}{Re} \nabla^2 v = 0,$$

$$\frac{\partial w}{\partial t} + u \frac{\partial w}{\partial x} + v \frac{\partial w}{\partial y} + w \frac{\partial w}{\partial z} + \frac{\partial p}{\partial z} - \frac{1}{Re} \nabla^2 w = 0,$$

(2)

$$\frac{\partial c}{\partial t} + u \frac{\partial c}{\partial x} + v \frac{\partial c}{\partial y} + w \frac{\partial c}{\partial z} - \frac{1}{Re} \nabla^2 c = 0,$$

(3)

where  $u$ ,  $v$ , and  $w$  are the components of the velocity in the  $x$ ,  $y$  and  $z$  directions, respectively,

and  $c$  is the mass concentration of the first fluid and Laplace operator  $\nabla^2 F = \frac{\partial^2 F}{\partial x^2} + \frac{\partial^2 F}{\partial y^2} + \frac{\partial^2 F}{\partial z^2}$ .

The boundary conditions are the no-slip and non-penetrating conditions at the stationary and moving walls.

Solutions of the incompressible Navier-Stokes system of partial differential equations with appropriate boundary conditions depend on a single parameter: the Reynolds number,  $Re = \rho UL/\mu$ , where  $\rho$  and  $\mu$  are density and viscosity of fluid respectively,  $U$  is the speed of cavity lid, and  $L$  is the length of cavity edge. For normalized variables used in the current study  $U$ ,  $L$  and  $\rho$  are taken equal to unity so that  $Re = 1/\mu$ .

To evaluate mixing quantitatively, the cavity is filled with two fluids having the same density and viscosity; therefore, the flow remains incompressible and controlled by a single parameter: the Reynolds number. The first fluid occupies the upper half of cavity ( $y > 0.5$ ), while the second fluid fills the lower half of cavity ( $y < 0.5$ ). Thus, the plane  $y = 0.5$  divides two species with the same properties, and the average value of concentration of each fluid in cavity is 0.5. The variance of concentration, that is, the degree of non-mixing of these two fluids, is quantified by the value of the mean square variable

$$\sigma^2 = \int (c - 0.5)^2, \quad (4)$$

where  $c(x, y, z, t)$  is the mass concentration of the first fluid computed by solving Eqn. (1-3).

When two fluids mix well with each other, the variable  $\sigma^2$  tends to zero. The standard deviation is the square root of the variance of concentration. This is another related measure of how spread out the concentration is.

At  $t=0$ , initial value of  $\sigma^2$  is equal to  $\sigma_0^2 = 0.25$  because the value of integrand is equal to  $(1-0.5)^2=0.5^2=0.25$  for the upper half of cavity and  $(0-0.5)^2=0.5^2=0.25$  for the lower half of cavity. The value of normalized deviation of concentration,  $\sqrt{\sigma^2/\sigma_0^2}$ , is plot in Figs. 2-4 as a function of unit-less time  $T=tU/L$ .

The 3-D cavity flowfield is obtained by the numerical solution of the three-dimensional viscous fluid flow equations (1-2), as described in the prior study of the author<sup>6</sup> by using ANSYS/Fluent finite-volume software with second-order upwind schemes for convective terms<sup>15,16</sup> and second-order central scheme for viscous terms. ANSYS/Fluent software uses the Semi-implicit Method for Pressure-linked Equations (SIMPLE)<sup>17</sup> to resolve velocity and pressure coupling in non-linear Navier-Stokes equations (Eqs. (2)). In Ref<sup>6</sup>, the grid convergence study for Case A is provided and comparison to prior literature solutions<sup>18,19,20</sup> for the benchmark Case C is included.

To evaluate grid-independence of the intensity of mixing, mixing rate for Case B1 was evaluated first for developing cavity flow initially at rest,  $(u,v,w)=0$  at  $t=0$ . Initial location of interface of two fluids is at  $y=0.5$ , where the first fluid occupies the upper region of cavity,  $y>0.5$ . The integral (4) was computed for the first ten units of normalized time for  $Re=2000$  and  $1000$ . The computed value of  $\sigma/\sigma_0$  is shown in Fig. 2.

The second cavity flow set-up corresponds to the injection of two fluids of equal density into developed cavity flow at  $T=10$ . As opposed to the prior situation, the mixing in this case occurs in fully-developed cavity flowfield. The initial location of interface of two fluids is at  $y=0.5$  as it was in the prior case. The integral (4) was computed for the first twenty units of normalized time after injection for  $Re=2000$  and  $1000$  as depicted in Fig. 2.

For the listed computations above, the implicit second-order temporal discretization method<sup>15</sup> is used with the time step  $\Delta t=0.01$ . Two uniform numerical grids with grid steps  $h=0.005$  ( $201 \times 201 \times 201$  grid) and  $h=0.01$  ( $101 \times 101 \times 101$  grid) are used to evaluate the grid independence of results. Present computational results show similar patterns of concentration variance for these grids; therefore, the  $201 \times 201 \times 201$  grid is selected for computations presented in the next sections. Studies<sup>21, 22</sup> show that the 3-D cavity flow (Case C) becomes unstable (transit to turbulence) when  $Re>2000$ . To limit the current study to stable flows,  $Re=2000$  is selected for the evaluation of mixing in the next sections.

### **3. Computational results**

For developing cavity flow, the mixing rate is slow for the first four time units, and practically the same for all considered cases, except for B2 (as depicted in Fig 3). For the latter case, the mixing starts relatively earlier, as both moving walls are relatively close to the interface of fluids near the upper left corner (see Fig 1c). For all other cases, the flowfield in the cavity has not been established yet to affect the interface.

Between the four and eight time units, the rate of mixing becomes different among considered cases (see Fig. 3). In particular, cases C, B3 and B1 appear to have slower mixing. For Case B3 (see Fig. 1d), the symmetry plane at  $y=0.5$  coincides with the interface of two mixing fluids. There is no flow across the symmetry line; therefore, there is no convection of species across the interface. For Case B1, the mixing rate is somewhat faster compared to the above cases; however,



the mixing rate becomes comparable to Case C towards the end of the considered time interval of ten units of time.

Cases B4 and A have substantially faster mixing rates compared to the cases listed above. Case A (Fig. 1a) is truly three-dimensional because the top and bottom walls of the cavity move in perpendicular directions. Case B4, in which the top and bottom walls of cavity move in opposite directions, has a stronger primary vortex compared to the benchmark Case C, in which only the top cavity wall moves. At ten time units, Cases B4 and A approach Case B2 in terms of completeness of mixing (see Fig. 3).

For comparison of mixing rates for developed cavity flow, the fully-developed cavity flowfield obtained in above computations is used as an initial condition. Initial location of interface of two fluids is at  $y=0.5$  as it were in the prior case. The value of  $\sigma/\sigma_0$  for all considered cases as a function of time is shown in Fig. 4 for 20 time units starting from injection of two fluids with their interface at  $y=0.5$ .

After considering all cases, it can be seen that the fastest mixing rate at every time moment occurs for Case A. Compare Fig. 5a to Fig. 6a to evaluate the flowfield in the central vertical cross-section for Cases A and C. While the 2-D vector flowfield projected on the central vertical plane seems qualitatively similar in both cases, the third component of velocity (perpendicular to the plane) makes mixing much faster for Case A. Starting from  $T=2$  (Fig. 5a), the interface for Case A is significantly more fractured; this leads to the formation of many smaller size areas of non-mixed fluids with a well-developed surface at later time moments (compare Figs 5b,c,d to Figs 6b,c,d). For Case C, the big unmixed area rotates with the circulating cavity flow (red area in Figs 6b,c,d,e).

At the end of the considered time interval, the mixing is closer to its completion for Case A in comparison to the mixing for Case C (compare Fig. 5e to Fig 6e).

In comparison to all considered cases, cases C, B1, and B2 (Figs. 6, 7 and 8, respectively) have medium mixing rates. For Case B1, the mixing at the mean diagonal plane is qualitatively similar to that for Case C (compare Figs. 7a and 6a) with substantial up-down flow along the front edge of the central diagonal plane. For Case B1, there is a significant flow in the plane perpendicular to the mean diagonal plane, which is directed inward the cavity and down of upper corners (see Fig. 7 a). Case B1 can be viewed as a set of 2-D cavities of variable length to depth ratios, from  $\sqrt{2}:1$  (mean diagonal plane) to  $0:1$  (near corners). Note that the flowfield within these cavities is connected by the flow in planes perpendicular to them. The mixing in the mean diagonal plane is relatively fast, as the corresponding 2-D cavity is shallow ( $\sqrt{2}:1$ ). However, the near-bottom part next to the off-diagonal corners of the cavity is slow-mixing, corresponding to the cavities being narrow and deep. The mixing for Case B1 is initially somewhat slower than that for baseline Case, while at  $T=20$ , the mixing rates for cases B1 and C become comparable.

For Case B2 (Fig. 8), the two fluids are initially separated by interface at  $y=0.5$ , while at later time moments, the diagonal plane of symmetry is created in a way that separates two fluids and slows down the mixing (see Fig. 8b,8c). At earlier time moments (see Fig. 8a), the transition of the interface between mixing fluids, from the horizontal to diagonal, creates a spiral motion and faster mixing. As a result, the mixing rate for Case B2 is the fastest at earlier times, and slows down at later time moments/as time progresses (see Figs. 8b,c ). While the mixing of two fluids in developed cavity flow is the fastest for Case A, the mixing in developing cavity flow is the fastest for Case B2.

Case B3 (Fig. 9) has the slowest mixing in comparison to all of the considered cases because of the formation of two symmetric vortices with respect to the plane  $y=0.5$ . Consequently, the mixing for Case B3 is caused mainly by diffusion, with the exception of 3-D effects in the plane perpendicular to the central vertical cross-section (as described in the next section).

Case B4 (Fig. 10) has the fastest mixing rate of the four cases listed above. Similar to Case C, the prominent up-down flow motion occurs along the right wall (see Fig. 6a and Fig. 10a). The flowfield for Case B4 has a strong down-up flow along the left wall, created by the motion of the bottom wall, while for Case C, the down-up flow is spread widely over the right half of the plane, and is relatively slow. For Case B4, big packets of unmixed fluid are formed at earlier time moments (Fig. 10a,b) and reduced to relatively narrow diagonal bands of non-mixed fluid at  $T=20$  (Fig. 10c). Therefore, the mixing rate is faster for Case B4 compared to Case C, and Case B4 is the second fastest (after Case A) in terms of mixing rate.

#### **4. Three-dimensional effects on mixing rate**

In Figure 11, the flowfield and concentration of species are shown in the vertical plane perpendicular to the axis  $x$  at  $x=0.5$  in order to depict the three-dimensional effects, including the finiteness of cavity in the  $z$  direction. The scale of velocity flow arrows is four times larger than those in Figs. 6-10a. For Case A, the moving cavity bottom in the  $z$  direction creates strong flow along the right edge in Fig. 11a. On the contrary, for Case C, the flow in this plane is relatively low except for the lower corners. The area with high concentration of the first fluid is formed near the centerline at the lower part of cavity ( $y<0.5$ ), while the area of high concentration of the second

fluid is formed near the top of the cavity. Along the side walls ( $z$  close to  $1$  or  $z$  close to  $0$ ), areas of higher concentration of the second fluid are formed at  $y \sim 0.5$  and  $y \sim 0.25$ . Compared to Case A, (compare Figs. 11a and 11b), the mixing is slower because packets of unmixed fluid are formed.

For Case B2, the interface between two fluids is formed at  $y \sim 0.5$ . The periodical vortical pattern and vertical flow component is formed along this interface, see Fig. 11c. The vertical flow component enhances convective mixing and forms local well-mixed regions of relatively small size (green areas in Fig. 11c). However, much larger areas of non-mixed first fluid (red area in Fig. 11c) and second fluid (blue area in Fig. 11c) are formed within top and bottom parts of cavity, respectively. Consequently, the mixing rate for Case B2 is slower compared to other considered cases except Case B3.

For Case B3 (depicted in Fig. 11d), the symmetry line is formed at  $y = 0.5$  (see previous section). Near the symmetry line, local flow regions are formed in a manner in which the flowfield is directed outward of the symmetry line; a couple of such areas appear within the cavity volume, and two regions are formed near the side walls of the cavity. While these flows enhance local convection and form green areas of completed mixing above and below the interface, the pairs of unmixed areas of an elliptic shape (dark red and dark blue) are formed in the interior of upper ( $y > 0.5$ ) and lower ( $y < 0.5$ ) regions of cavity. The formation of unmixed zones and slow convection across the interface confirms the slowest mixing rate for Case B3 compared to the other considered cases (see Fig. 11d).

For Case B4 (Fig. 11e), the central elongated and partially-mixed (yellow) area with vertical flowfield is surrounded by unmixed (red) peripheral area. Relatively strong vortices are formed near the bottom in the central part (green and yellow mixed areas) and at the bottom corners. The formation of these vortices assist in causing the fastest mixing rate for Case B4 compared to other considered cases, except that for Case A.

## **Conclusions**

In this study, the mixing rate is evaluated for six different set-ups of moving 3-D wall-driven cavity flows. The set-ups include the cavity with its top and bottom walls moving in perpendicular directions (Case A), the cavity with its lid moving within its plane along its diagonal (Case B1), the cavity with its top and one of its side vertical walls moving in perpendicular directions (Case B2), the cavity in which the top and bottom walls move parallel to each other (Case B3), and the cavity in which its top and bottom walls move in opposite directions (Case B4). The mixing rates for the cases listed above are compared to the baseline lid-driven cavity flow (Case C). The mixing of two fluids of equal density and viscosity initially occupying the upper and lower halves of cavity is modeled numerically so that the variance of concentration is computed as a function of time.

The intensity of mixing was evaluated for developing cavity flow, which was initially at rest, for ten time units and for twenty time units. For the developing cavity flow, the mixing rate is fastest for Case B2. Other cases have quite similar mixing rates for their respective first four time units; specifically, the cases are categorized as faster-mixing cases for B4 and A, and slower-mixing cases for B1, C, and B3.

For the developed cavity flow, the mixing rate is the fastest for Case A followed by Case B4. The baseline Case C has a faster mixing compared to B4 from  $T \approx 7$  to  $T \approx 14$  units; however, for  $T > 14$  Case B4 has a faster mixing rate. Other cases (B1, B2 and B3) have slower mixing rates compared to Case C's mixing rate. Case B1 has a faster mixing rate compared to B2's mixing rate for  $T \geq 12$ . Case B3 has the slowest mixing rate at all times.

The interface between two fluids for the substantially 3-D Case A is significantly more fractured compared to the interface between two fluids for Case C. The genuinely 3-D flow in Case A leads to the formation of many smaller size areas of non-mixed fluids, which causes faster mixing. Case B4 has a relatively fast mixing rate compared to Case C's mixing rate because of stronger rotational motion in the  $(x, y)$  plane. In addition, 3-D effects, such as the formation of vortices in the  $(z, y)$  plane, speed-up mixing.

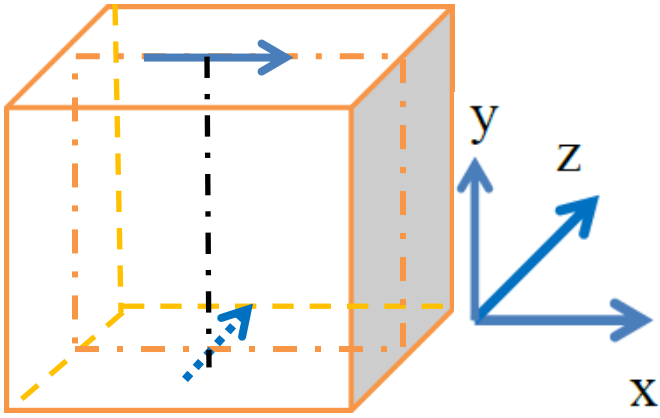
Case B1 has a somewhat slower mixing rate compared to Case C; nevertheless, the mixing rate becomes comparable in these two cases when mixing time approaches 20 units. For Case B1, mixing at the central diagonal rectangular cavity, which is relatively shallow,  $\sqrt{2}:1$ , is more intensive compared to the squared  $(x, y)$  cavity for Case C. However, for Case B1 mixing in off-diagonal cavities with larger depth-to-length ratios is relatively slow. The 3-D flow in the direction normal to the diagonal lid motion softens the above difference in mixing making it comparable to the baseline Case C.

Case B2 has the fastest mixing rate during the 10 units after the swift beginning of motion of the top and left cavity walls. Later, symmetrical flowfield is formed with respect to the cavity diagonal

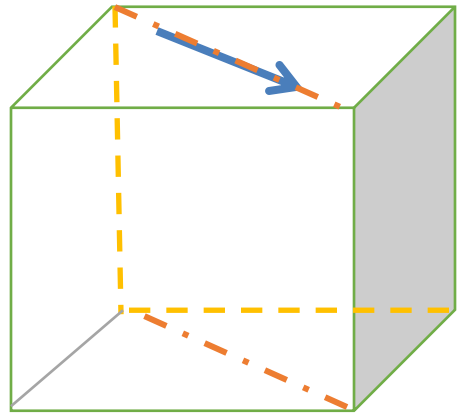
plane passing through the upper left corner. The transition of the interface between mixing fluids from the horizontal (at  $y=0.5$ ) to diagonal plane of symmetry creates a fast mixing rate for two fluids. The mixing rate substantially slows down as soon as diagonal symmetry has formed. Near the interface of two fluids, local flow regions are formed in the  $(y, z)$ -plane in which the flowfield is directed outward of horizontal interface; thus, increasing the mixing rate.

Case B3 has the slowest mixing rate at all times. During the first 10 units after start of developing flow, the rate of mixing is comparable to the baseline Case C, followed by slower mixing after the symmetry plane  $y=0.5$  has formed.

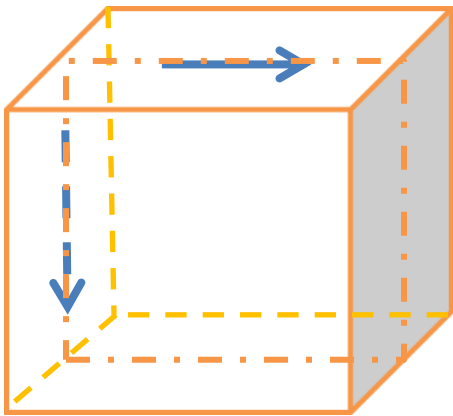
The presented evaluation of flow mixing intensity and rates for the various arrangements of moving cavity walls will assist in the evaluation of mixing in enclosures with moving and stationary parts.



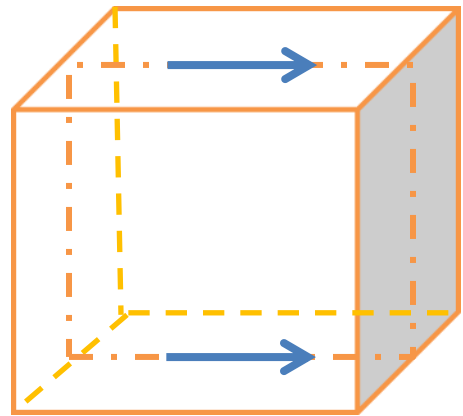
(a)



(b)

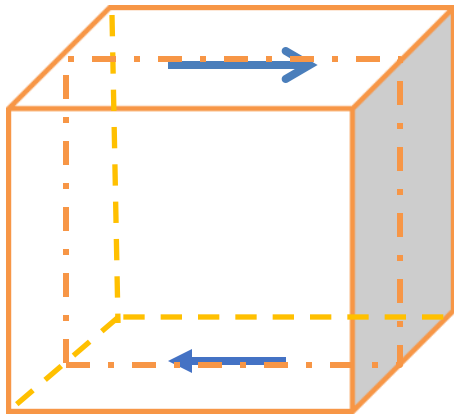


(c)

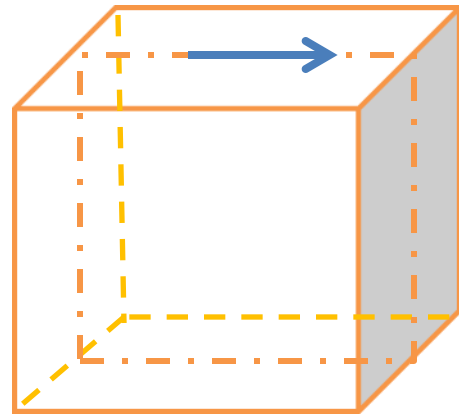


(d)





(e)



(f)

Figure 1: Flows induced by moving walls of cubical cavity: (a) top and bottom walls move in perpendicular directions (Case A), (b) top wall moves along its diagonal (Case B1), (c) top wall moves along the x direction and the left wall moves down in the negative y direction (Case B2), (d) top and bottom walls move parallel (Case B3), (e) top and bottom walls are in reverse motion (Case B4) and (f) top wall moves along its edge (Case C). The central vertical plane is shown in which flowfield and concentration are depicted.

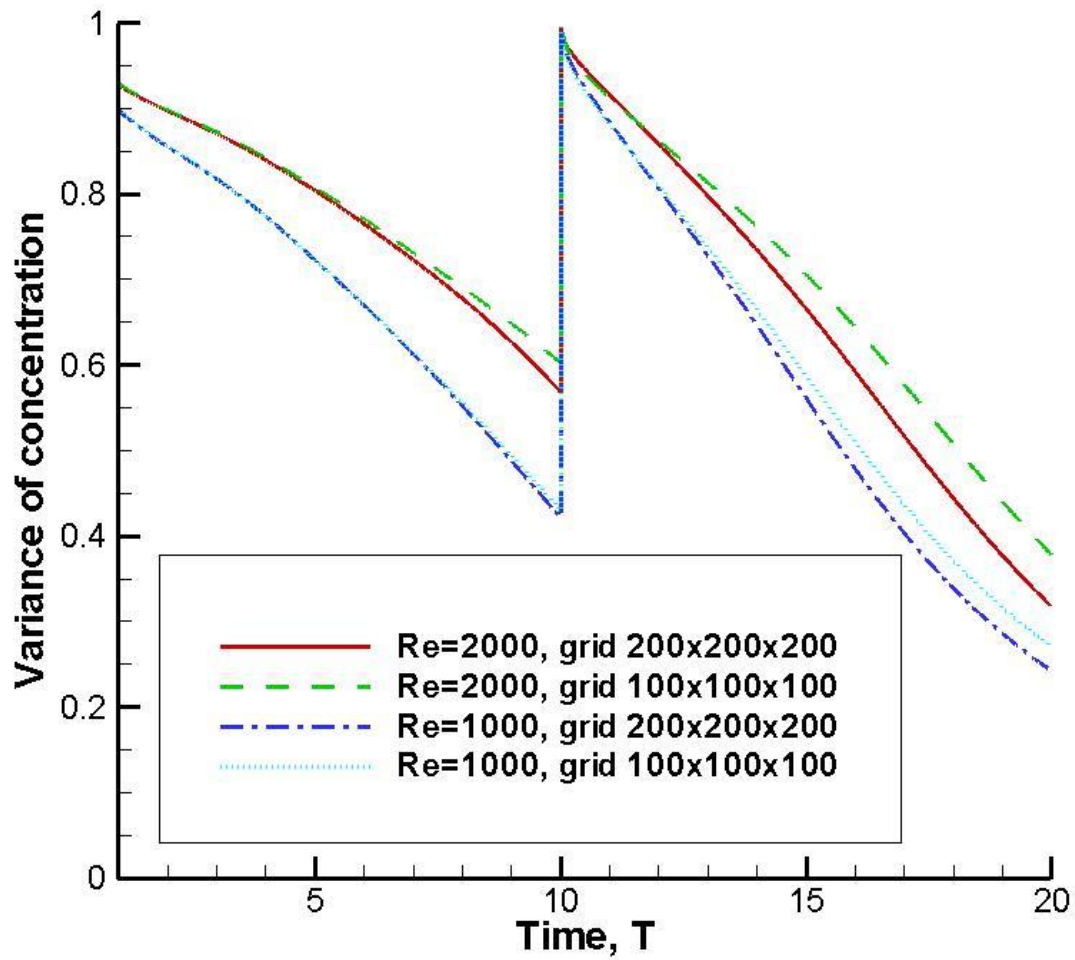


Figure 2: Mixing variance,  $\sigma$ , for Case B,  $Re=1000$  and  $2000$ . Finite-volume grids  $200^3$  and  $100^3$  are used.

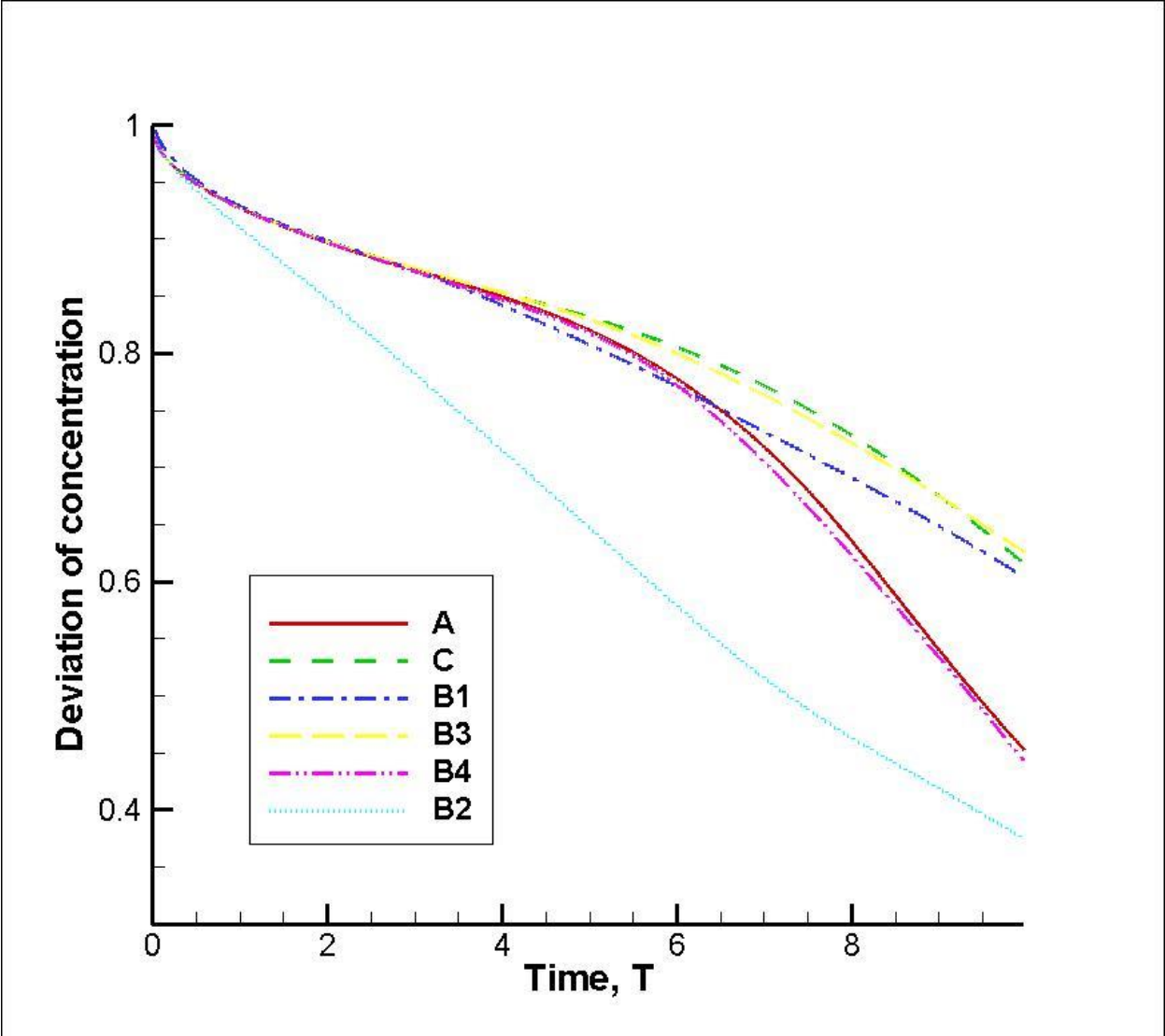


Figure 3: Mixing variance for transient cavity flow

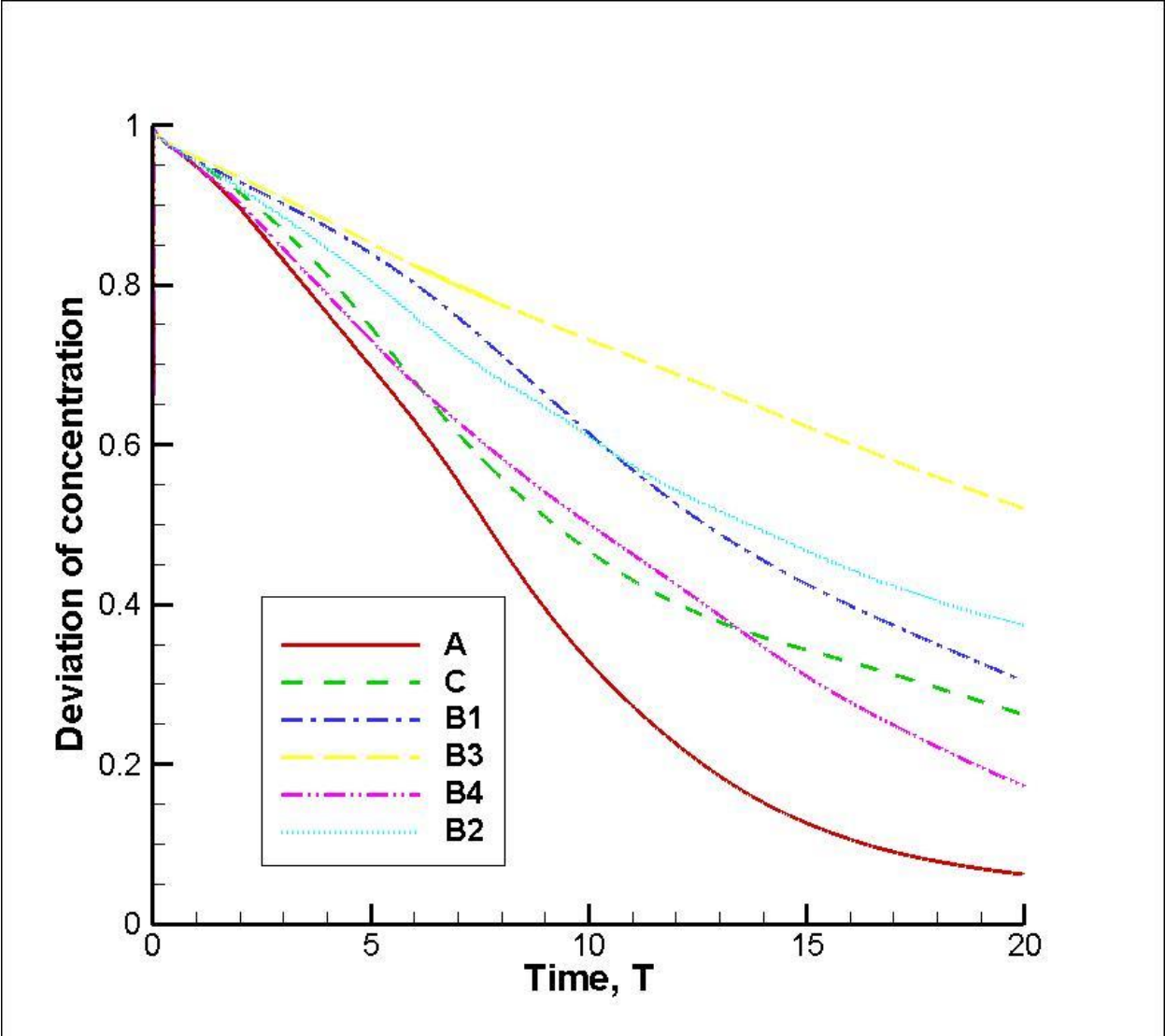
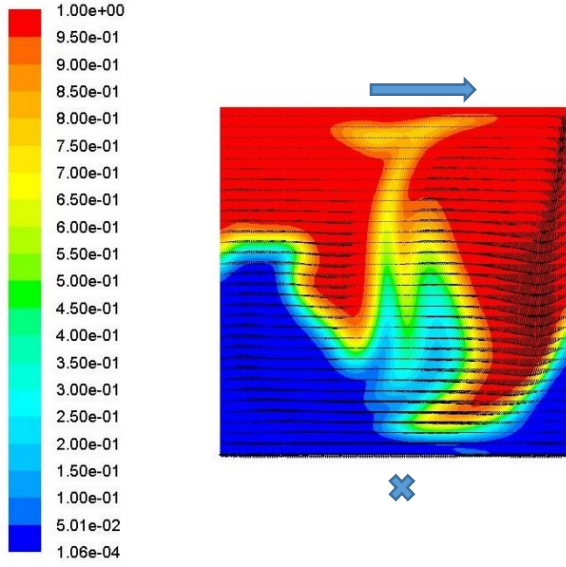
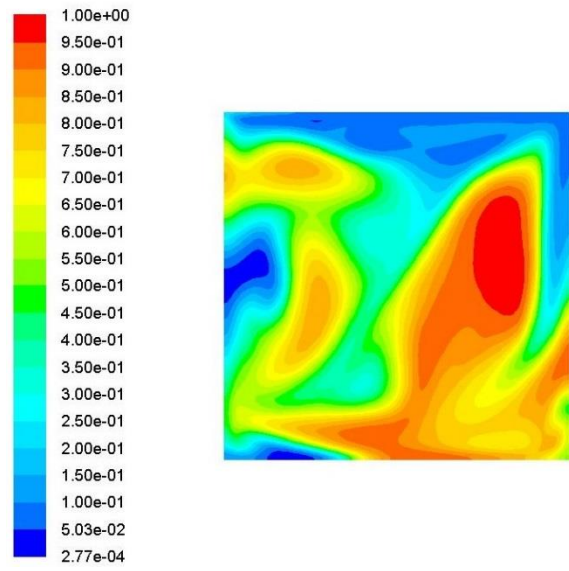


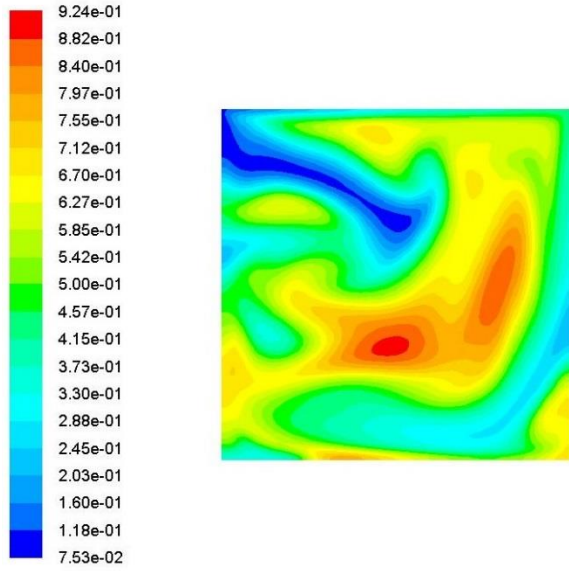
Figure 4: Mixing variance for developed cavity flow



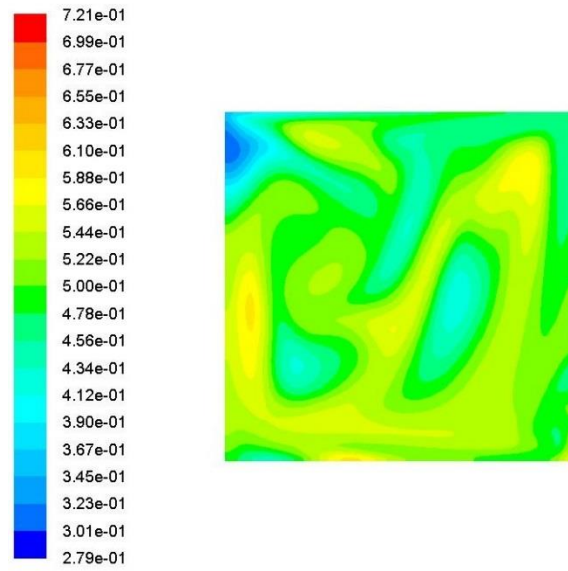
(a)



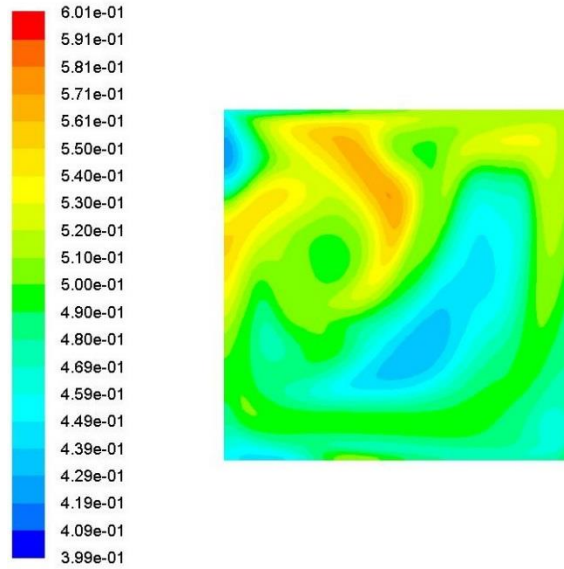
(b)



(c)



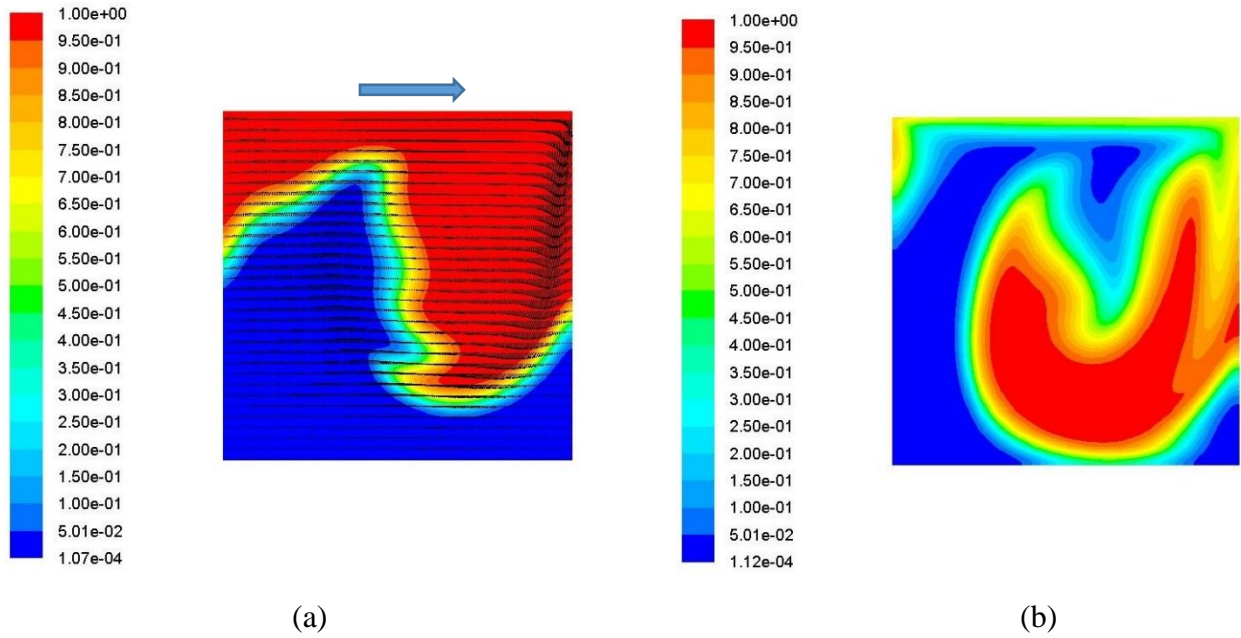
(d)



(e)

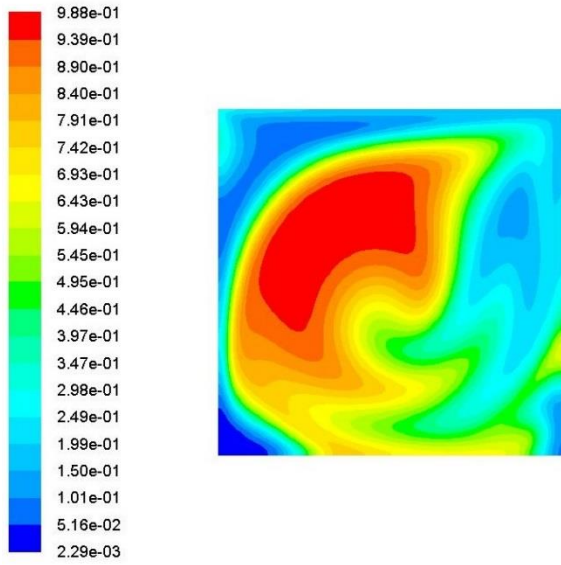
Figure 5: Case A: concentration of first fluid at time moments (a) 2, (b) 6, (c) 10, (d) 16, and (e) 20 units after injection into developed flow. Velocity vector field is shown in (a).

⊗ is the moving wall direction perpendicular to the figure plane directed toward the back.

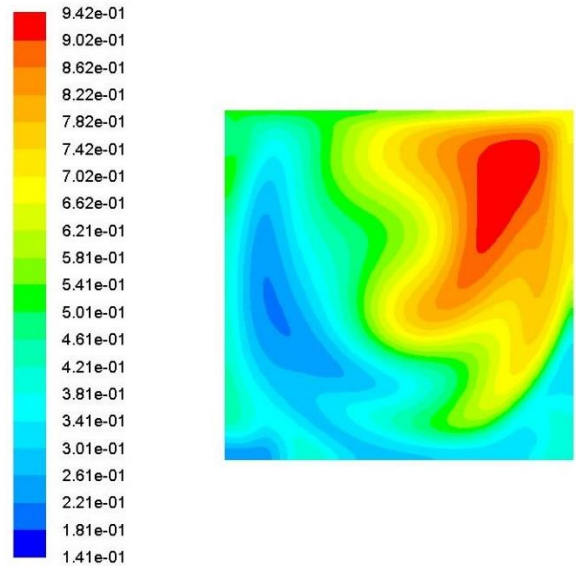


(a)

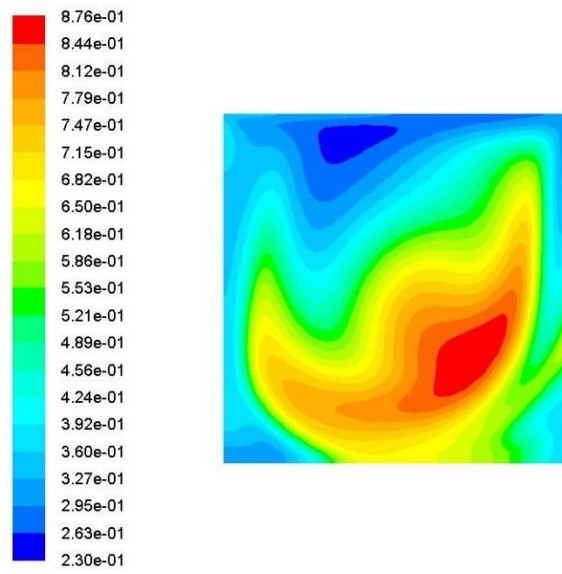
(b)



(c)



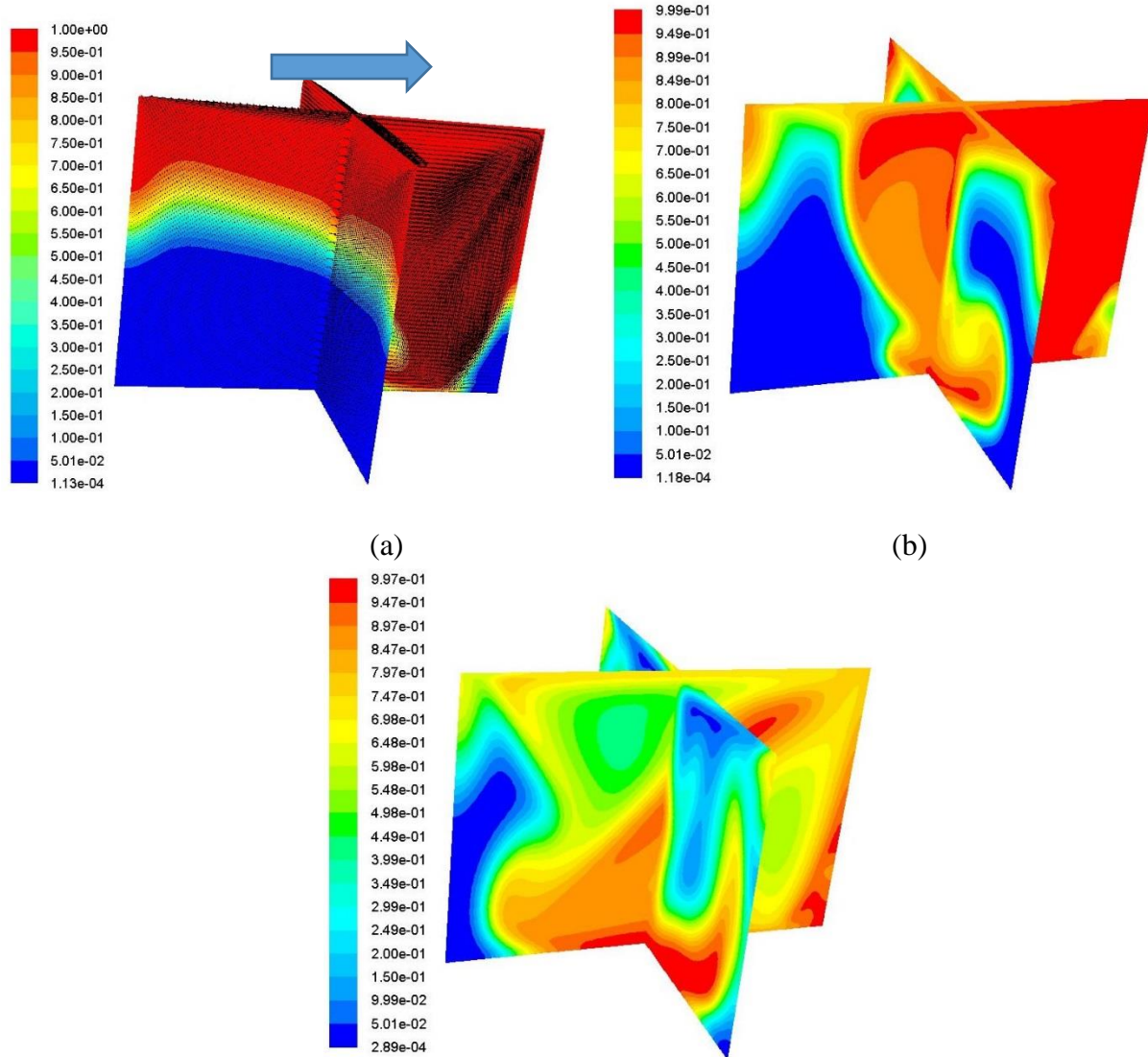
(d)



(e)

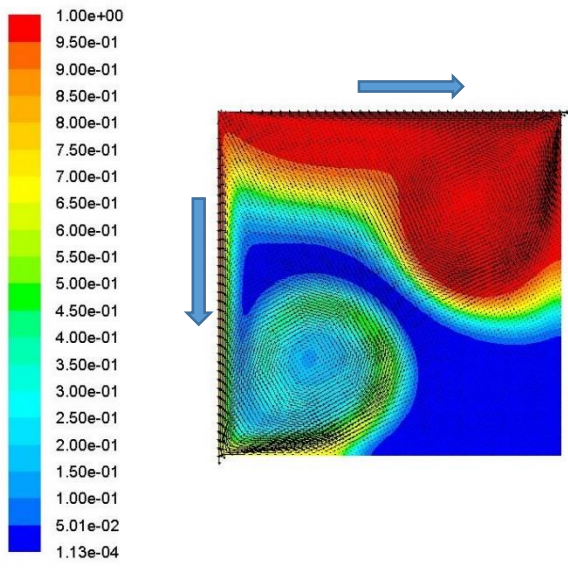
Figure 6: Case C. Conditions are the same as in Fig. 5



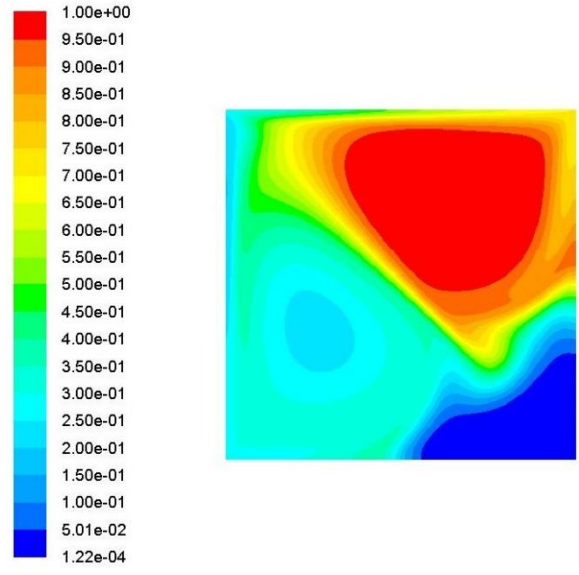


(a) (b) (c)  
 Figure 7: Case B1: concentration of first fluid at (a) 5, (b) 10, and (c) 20 time units after injection into developed flow. Velocity vector field is shown in (a).

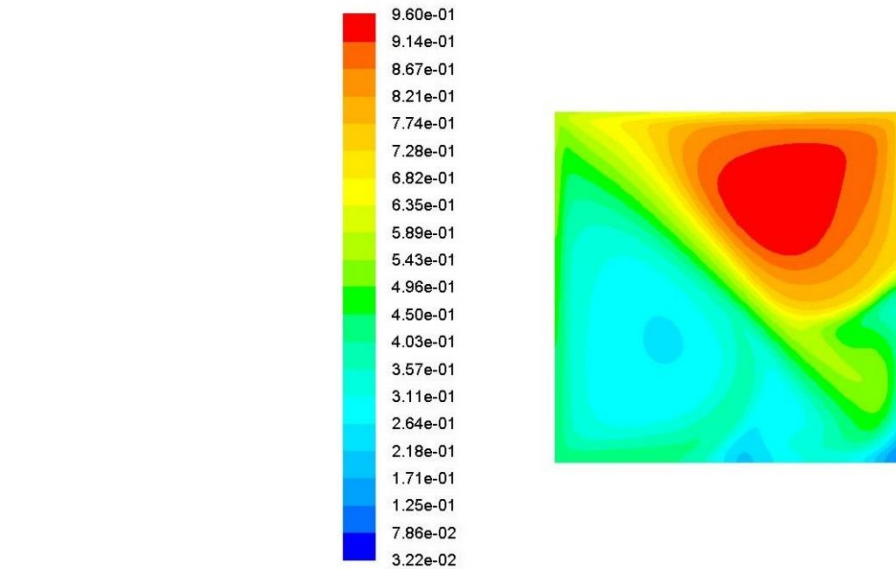




(a)

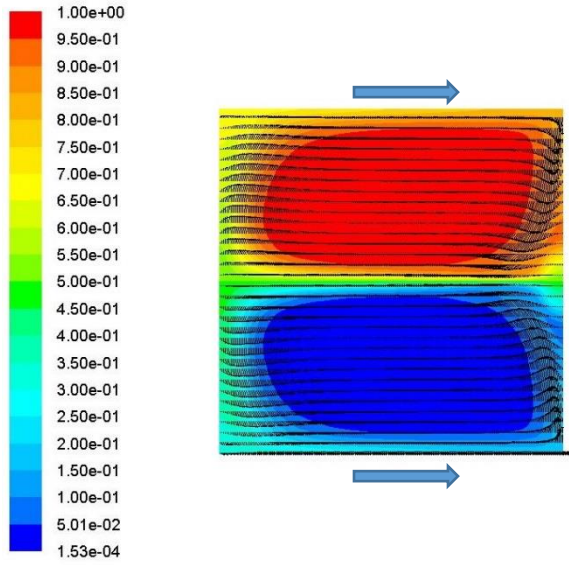


(b)

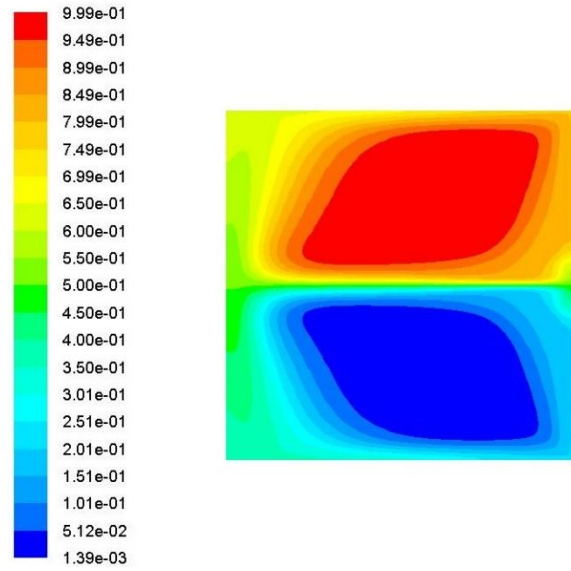


(c)

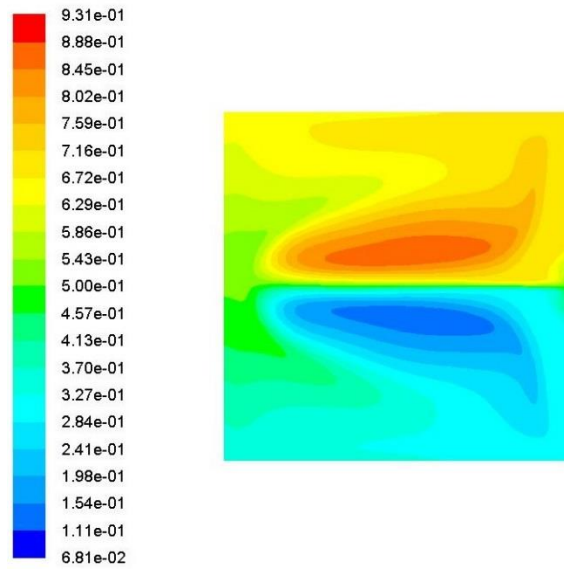
Figure 8 Case B2. Conditions are the same as in Fig. 7.



(a)



(b)



(c)

Figure 9: Case B3. Conditions are the same as in Fig. 7.

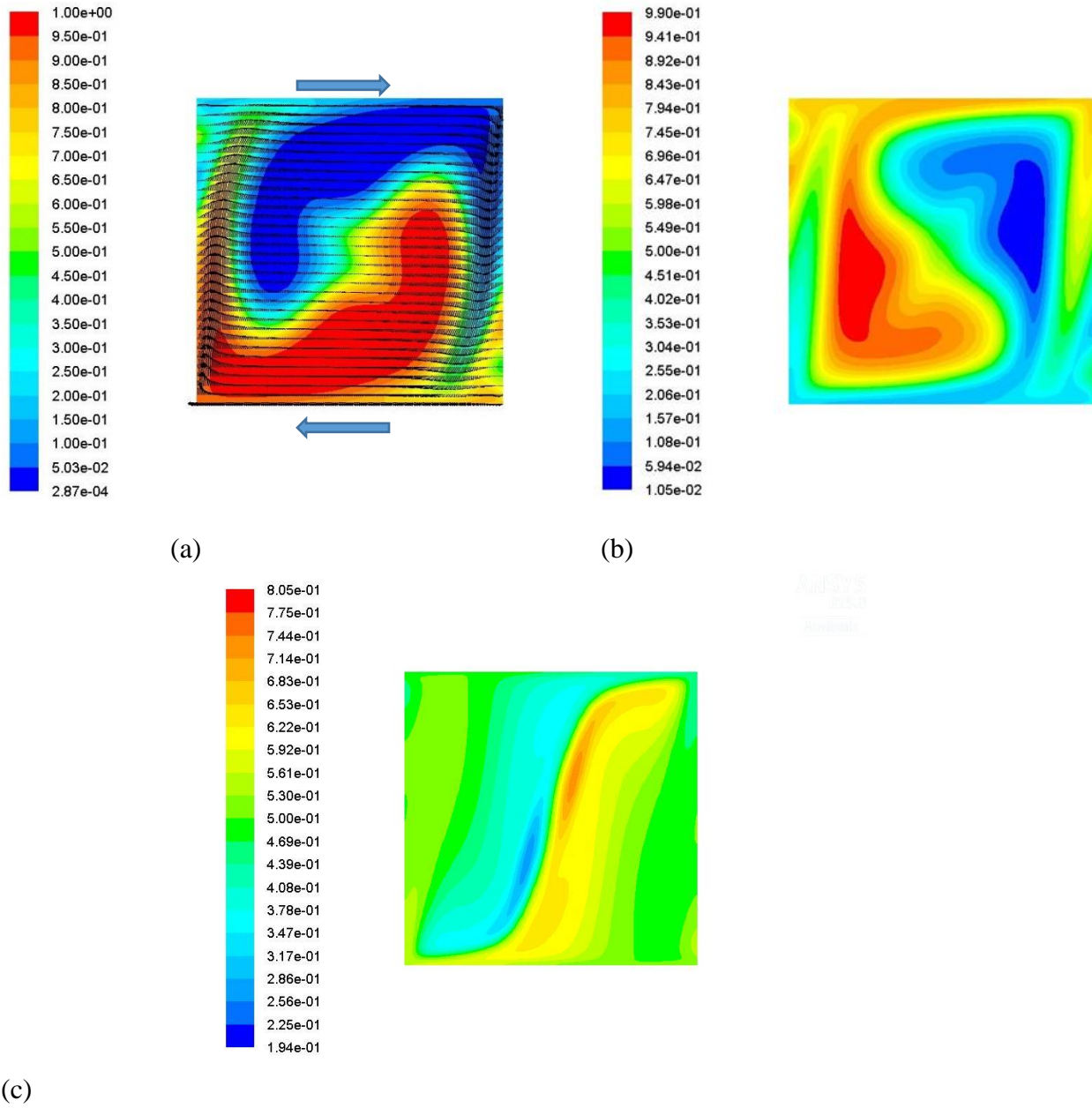
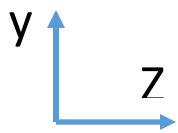
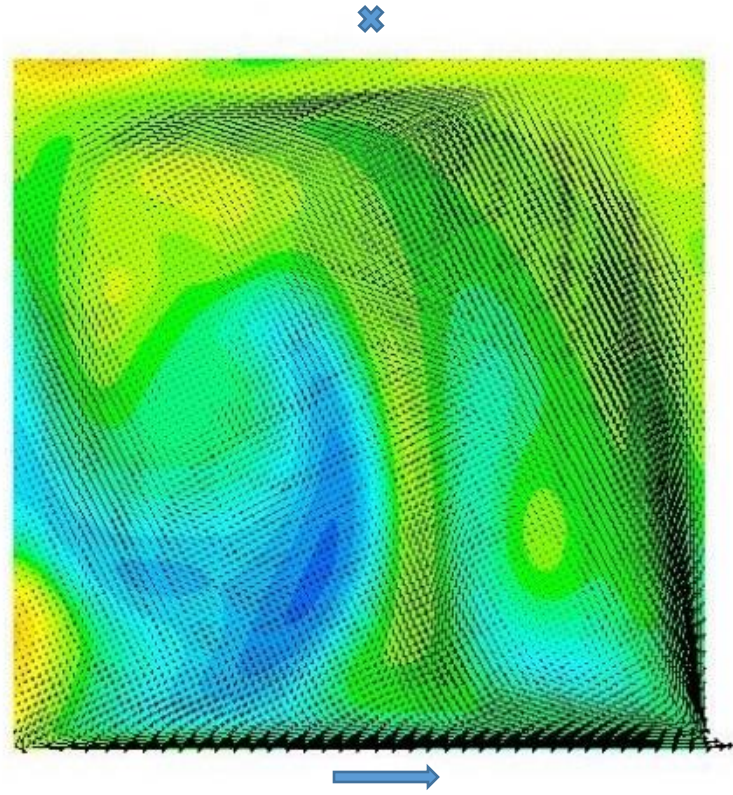
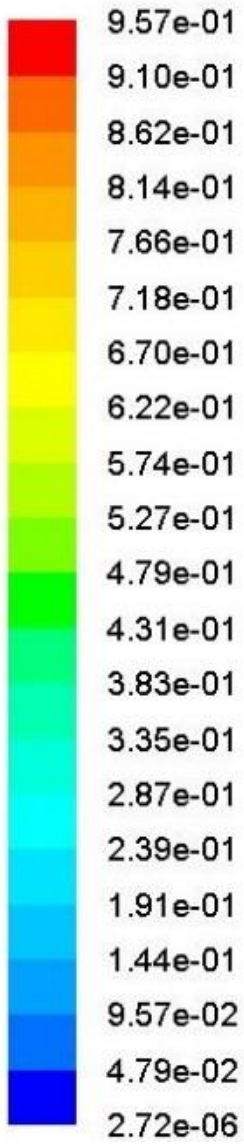
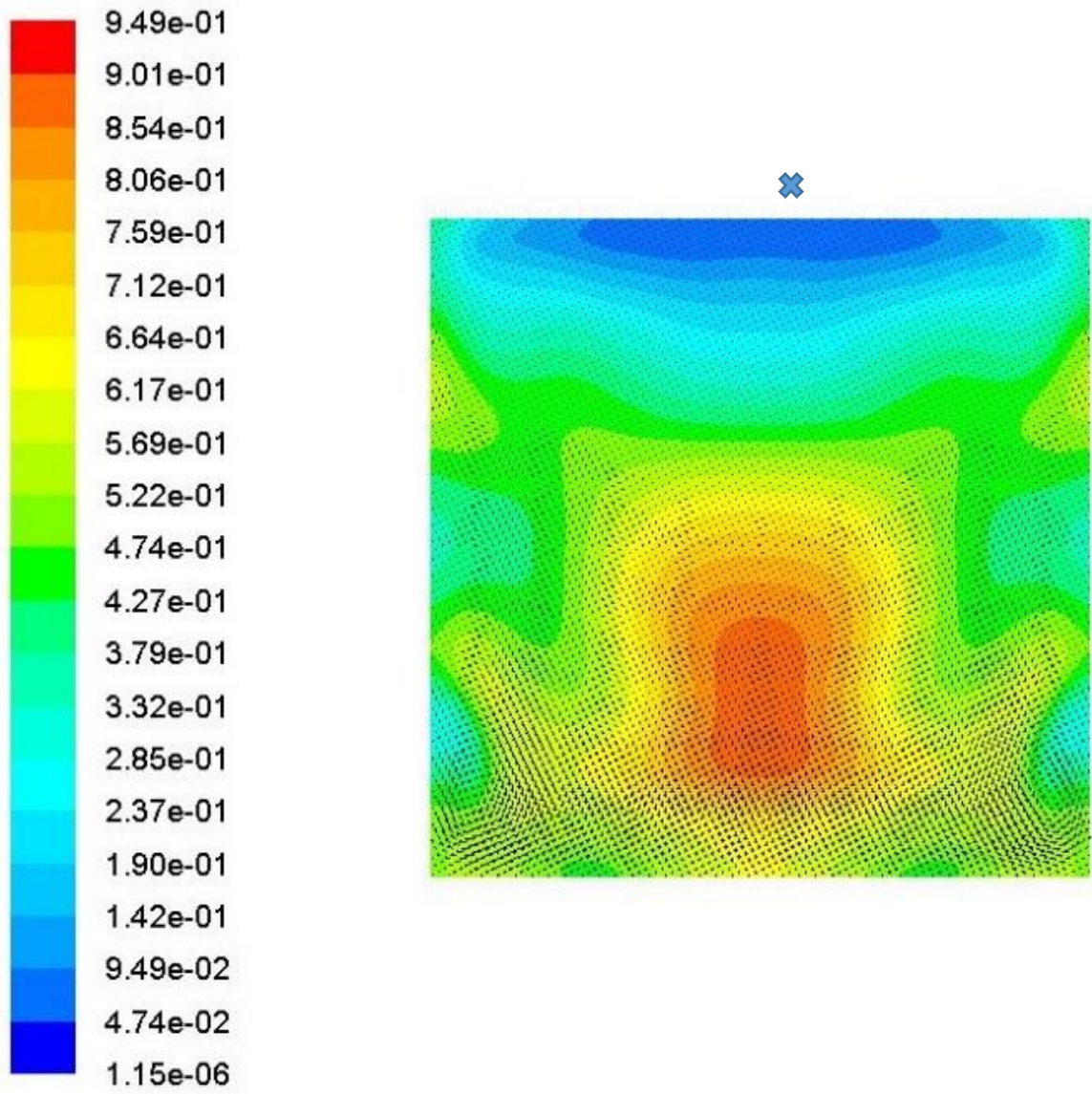


Figure 10: Case B4. Conditions are the same as in Fig. 7.

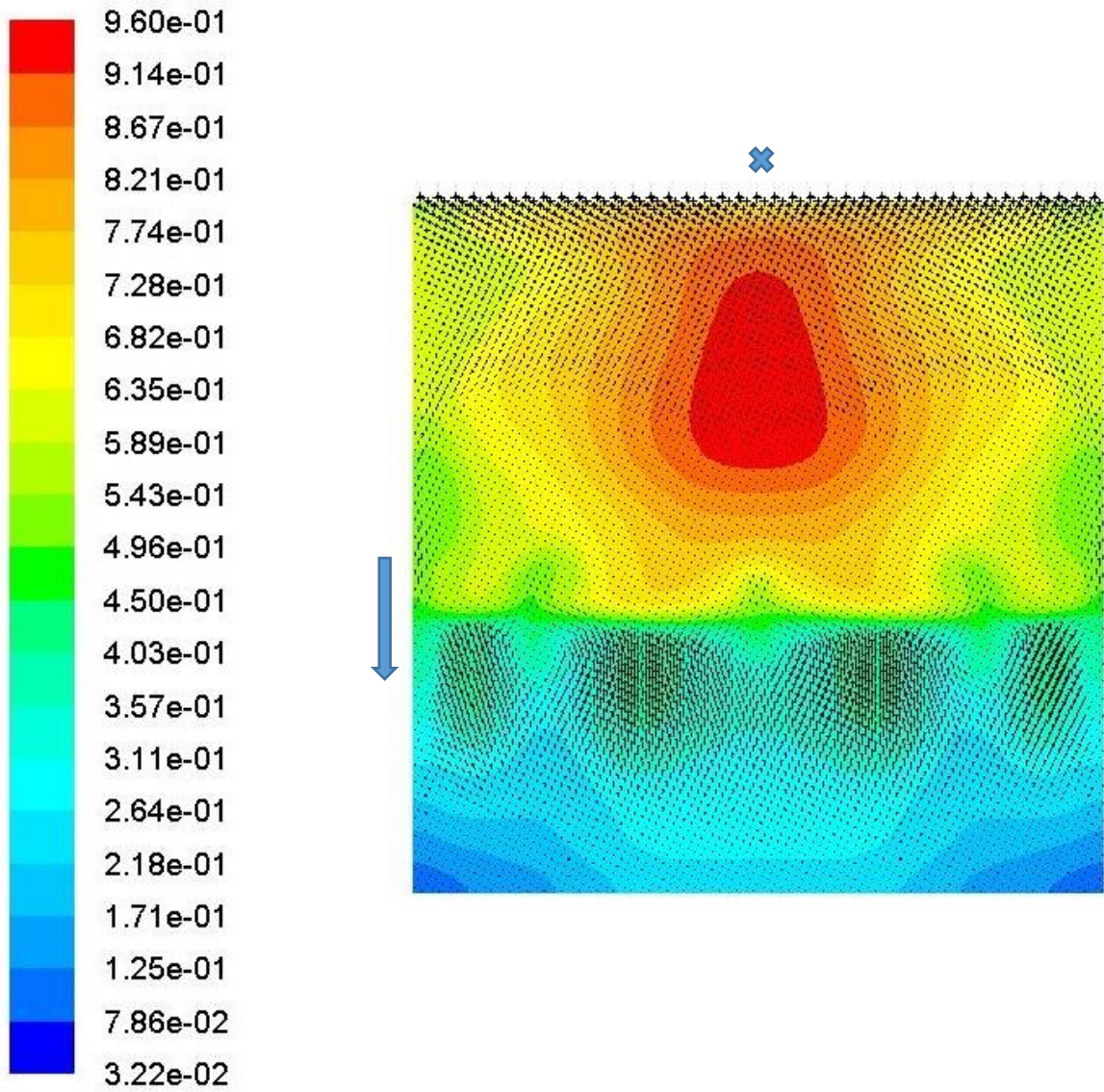


(a)

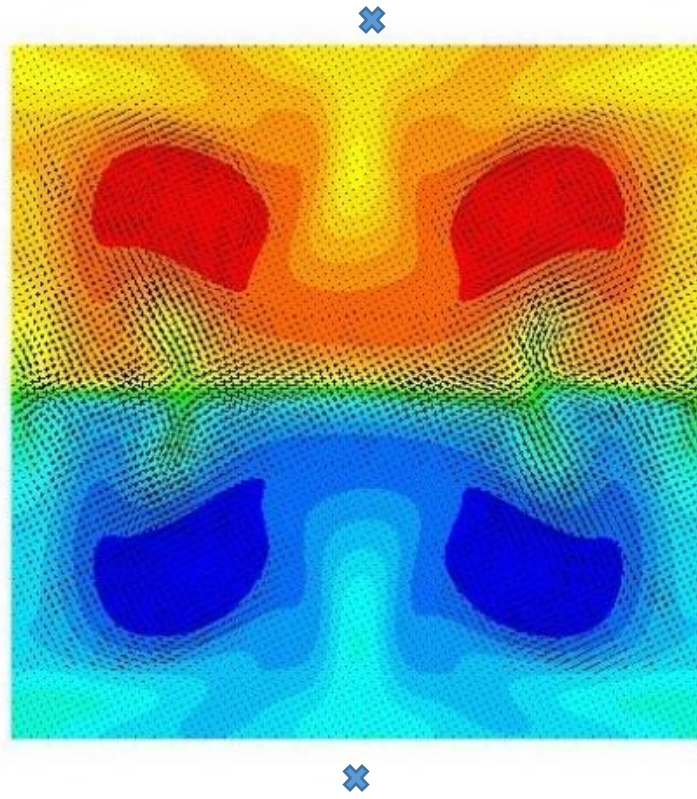
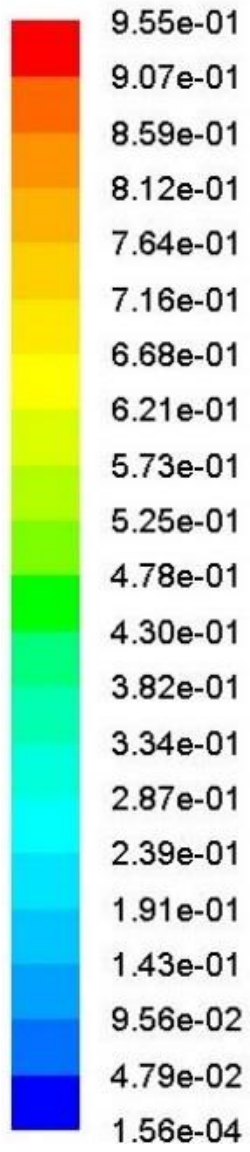




(b)

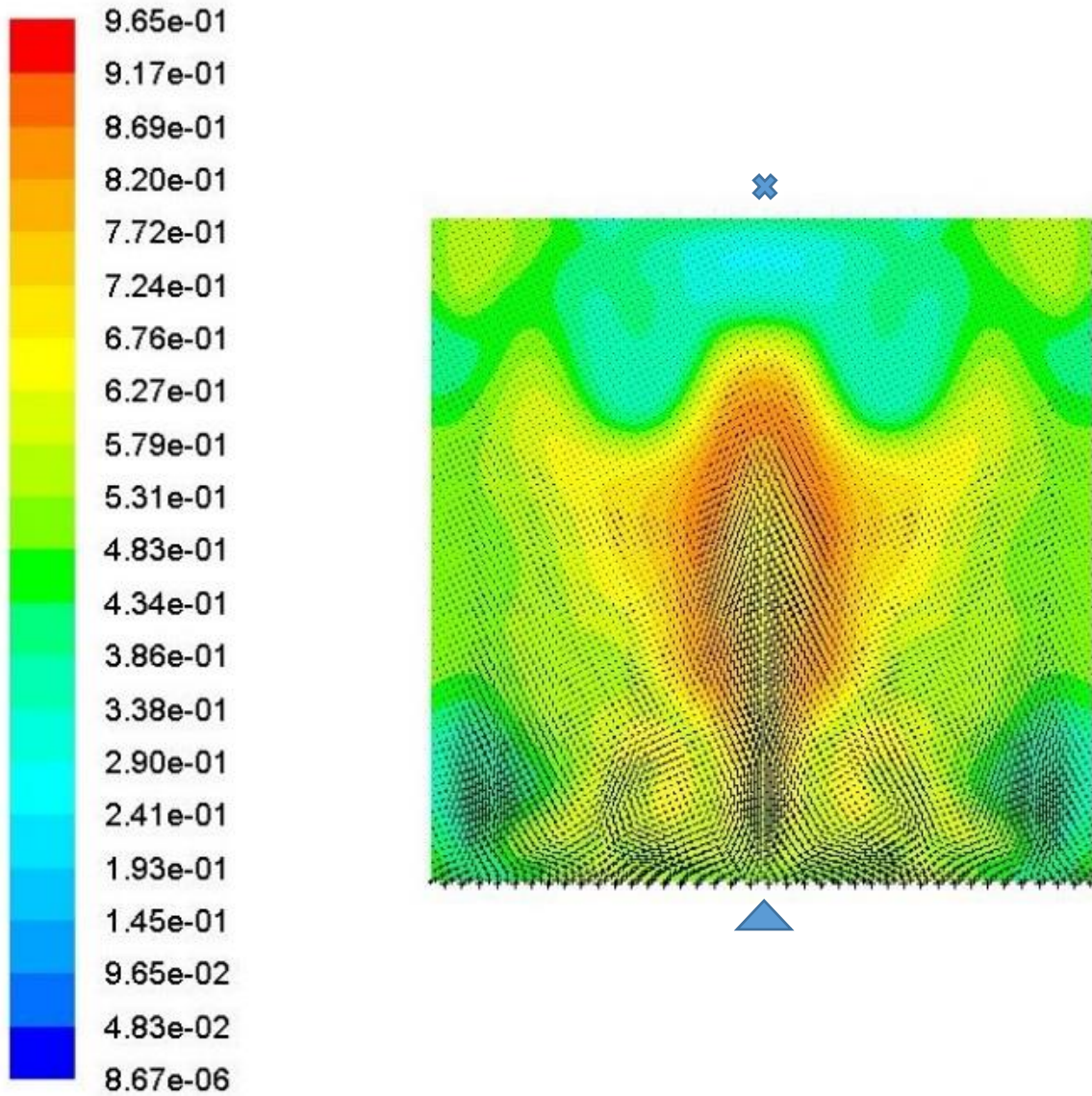


(c)



(d)





(e)

Figure 11: Concentration and flowfield in vertical plane: (a) Case A, (b) Case C, (c) Case B2, (d) Case B3, and (e) Case B4.

✘ is the moving wall direction perpendicular to the figure plane directed toward the back,  
 ▲ is the moving wall direction directed toward the front.



## References

---

- <sup>1</sup> P. N. Shankar and M. D. Deshpande, Fluid mechanics in the driven cavity, *Ann. Rev. Fluid Mech.*, 2000, Vol. 32, pp. 93–136.
- <sup>2</sup> J. R. Koseff and R. L. Street, On end wall effects in a lid-driven cavity flow, *ASME Journal of Fluids Engineering*, 1984, Vol. 106, pp. 385-389.
- <sup>3</sup> C. Migeon, A. Texier, and G. Pineau, Effects of lid-driven cavity shape on the flow establishment phase, *Journal of Fluids and Structures*, 2000, Vol. 14, pp. 469-488.
- <sup>4</sup> S. Middleman, *Fundamentals of Polymer Processing*, 1977, New York: McGraw Hill.
- <sup>5</sup> K. L. McIlhany, D. Mott, E. Oran, and S. Wiggins, Optimizing mixing in lid-driven flow designs through predictions from Eulerian indicators, *Physics of Fluids*, 2011, Vol. 23, p. 082005.
- <sup>6</sup> A. Povitsky, Three-dimensional flow with elevated helicity in driven cavity by parallel walls moving in perpendicular directions, *Physics of Fluids*, 2017, Vol. 29, p. 083601.
- <sup>7</sup> A. Povitsky, Three-dimensional flow in cavity at yaw, *Nonlinear Anal. Theory Methods Appl.* 2005, Vol. 63, pp. e1573–e1584. Preliminary versions: AIAA Paper 2847-2001, Tech. Rep. 211232, NASA/CR (2001), *ICASE Report* No. 2001-31.
- <sup>8</sup> Y.-H. Ryu and J.-J. Baik, Flow and dispersion in an urban cubical cavity, *Atmospheric Environment*, 2009, Vol. 43, Issue 10, pp. 1721–1729.
- <sup>9</sup> P. Kosinski, A. Kosinska, and A.C. Hoffmann, Simulation of solid particles behavior in a driven cavity flow, *Powder Technology*, 2009, Vol. 191, Issue 3, pp. 327–339.
- <sup>10</sup> B. B. Beya and T. Lili, Three-dimensional incompressible flow in a two-sided non-facing lid-driven cubical cavity, *C. R. Mecanique*, 2008, Vol. 336, p. 863.
- <sup>11</sup> F. Oueslati, B. Ben Beya, and T. Lili. Aspect ratio effects on three-dimensional incompressible flow in a two-sided non-facing lid-driven parallelepiped cavity. *C. R. Mecanique*, 2011, Vol. 339, pp. 655–665.
- <sup>12</sup> S. Arun and A. Satheesh, Analysis of flow behavior in a two sided lid driven cavity using Lattice Boltzmann technique, *Alexandria Engineering Journal*, 2015, Vol. 54, pp. 795–806.
- <sup>13</sup> F. Romanò, S. Albensoeder and H. C. Kuhlmann, Topology of three-dimensional steady cellular flow in a two-sided anti-parallel lid-driven cavity, *Journal of Fluid Mechanics*, 2017, Vol. 826, pp. 302-334.
- <sup>14</sup> S. S. Mendu and P.K. Das, Flow of power-law fluids in a cavity driven by the motion of two facing lids – A simulation by lattice Boltzmann method, *Journal of Non-Newtonian Fluid Mechanics*, 2012, Vol. 175-176, pp. 10–24.
- <sup>15</sup> ANSYS Fluent guide, ANSYS Inc., Version 2018, PDF Documentation, 2018.
- <sup>16</sup> T. Barth and J. Jespersen "The design and application of upwind schemes on unstructured meshes", AIAA-89-0366, AIAA 27th Aerospace Sciences Meeting, Reno, Nevada, 1989.
- <sup>17</sup> Patankar, S. Numerical heat transfer and fluid flow. CRC press, 1980.

- 
- <sup>18</sup> B. Jiang, T.L. Lin and L. A. Povinelli, Large-scale computation of incompressible viscous flow by least-squares finite element method, *Comput. Methods Appl. Mech. Engrg.* 1994, Vol. 114, pp. 213-231.
- <sup>19</sup> G. Guy and F. Stella, A Vorticity-Velocity Method for the Numerical Solution of 3D Incompressible Flows, *Journal of Computational Physics*, 1993, Vol. 106, pp. 286-289.
- <sup>20</sup> J.-Y. Yang, S.-C. Yang, Y.-N. Chen, and C.-A. Hsu, Implicit Weighted ENO Schemes for the Three-Dimensional Incompressible Navier–Stokes Equations, *Journal of Computational Physics*, 1998, Vol. 146, pp. 464–487.
- <sup>21</sup> R. Iwatsu, K. Ishii, T. Kawanura, and K. Kuwahara, Numerical simulation of three-dimensional flow structure in a driven cavity,” *Fluid Dyn. Res.*, Vol. 5, 1989, pp. 173-189.
- <sup>22</sup> F. Giannetti , P. Luchini, and L. Marino, Linear stability analysis of three-dimensional lid-driven cavity flow, *Atti del XIX Congresso AIMETA di Meccanica Teorica e Applicata*. Aras Edizioni Ancona, Italy, 2009. See [http://www.dipmat.univpm.it/aimeta2009/Atti%20Congresso/SESSIONI SPECIALI/Marino\\_paper277.pdf](http://www.dipmat.univpm.it/aimeta2009/Atti%20Congresso/SESSIONI%20SPECIALI/Marino_paper277.pdf) , retrieved 05/20/2018